ORGANOMETALLICS

Article

pubs.acs.org/Organometallics

Electron-Rich Arene–Ruthenium Metalla-architectures Incorporating Tetrapyridyl–Tetrathiafulvene Donor Moieties

Vaishali Vajpayee,[†] Sébastien Bivaud,[†] Sébastien Goeb,[†] Vincent Croué,[†] Magali Allain,[†] Brian V. Popp,[‡] Amine Garci,[§] Bruno Therrien,*[,§] and Marc Sallé*[,†]

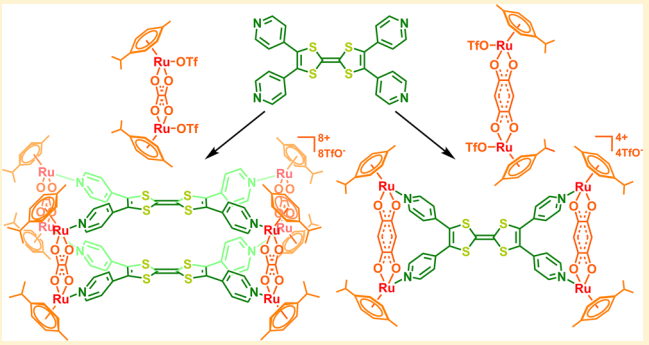
[†]Laboratoire MOLTECH-Anjou, Université d'Angers, CNRS UMR 6200, , 2 Boulevard Lavoisier, 49045 Angers Cedex, France

[‡]Eugene Bennett Department of Chemistry, West Virginia University, PO Box 6045, Morgantown, West Virginia, United States

[§]Institute of Chemistry, Université de Neuchâtel, Avenue de Bellevaux 51, CH-2000, Neuchâtel, Switzerland

Supporting Information

ABSTRACT: A series of arene ruthenium architectures have been prepared from coordination-driven self-assembly using dinuclear *p*-cymene ruthenium acceptors and π-donating tetratopic tetrapyridyl–tetrathiafulvalene donor ligands. The synthetic strategy, based on a geometric interaction approach, leads to four electroactive metalla-assemblies, **1**–**4** (one molecular cube and three metallaplates), that were characterized by NMR, ESI-MS, X-ray diffraction, and cyclic voltammetry. Rationalization of their formation discrepancy was completed by DFT calculations supported by structural features of their constituting TTF and Ru-complex components. Metalla-architectures possessing electron-rich cores (**3**, *cis*-**4**, and *trans*-**4**) interact strongly with picric acid (PA) to yield cocrystallized products, PA + metalla-assemblies, confirmed by single-crystal X-ray structure analyses.



INTRODUCTION

In the last decades, supramolecular coordination-driven assembly has emerged as a remarkable tool to design intricate molecular architectures.[1] In particular, donor–acceptor coordination-driven assembly has provided a sophisticated and efficient way to construct nanosized metalla-architectures with well-defined shape and size, structures otherwise inaccessible by conventional routes.[2] Metalla-architectures assembled from arene ruthenium building blocks are particularly attractive due to their interesting functions and potential applications in various areas of chemistry, including host–guest chemistry, catalysis, chemotherapy, and photo- and electrochemical sensing.[3]

The electron-donating tetrathiafulvalene moiety (TTF) has received a great deal of attention and constitutes a major component of various conducting materials,[4] sensors, and switches.[5] The incorporation of TTF in these systems is rationalized by a well-defined electrochemical behavior of TTF derivatives, which can be easily and reversibly oxidized into their corresponding cation radicals ($TTF^{\bullet+}$) and dications (TTF^{2+}). On this ground, integrating the TTF backbone within host structures may favor the recognition of electron-poor substrates.

Despite numerous studies dealing with the synthesis of TTF-based derivatives[6] and TTF-based ligands,[5,7] the preparation of discrete self-assembled architectures from a TTF backbone remains relatively unexplored. Recently, we introduced the first metallacycles and -cages built from side panels incorporating TTF moieties,[8,9] namely, bispyrollo(tetrathiafulvalene) (BPTTF) and the so-called extended-tetrathiafulvalene (exTTF). It is worth noting that these assemblies were obtained with square-planar Pt(II) or Pd(II) complexes.

Herein, we present the first examples of coordination-driven self-assembled metalla-architectures involving the parent TTF core. This has been made possible by the synthesis of the tetratopic tetrapyridyl-TTF isomeric ligands **L1** (tetra(4-pyridyl)TTF) and **L2** (tetra(3-pyridyl)TTF). As already shown with alternative isomeric compounds bearing 4- and 3-pyridyl coordinating groups, highly distinctive discrete structures may be expected from the same metal complex along the self-assembly process.[10] Moreover, in the present work, the metal complex corresponds to arene ruthenium acceptors of identical bite angle but involving distinctive lengths. Therefore, this report addresses the effect of the crossed influence between the ligand geometry (3- and 4-pyridyl derivatives) and the length of the dinuclear Ru-based acceptor, relative to the structure of the resulting assemblies. These results were supported by DFT calculations. Along with the synthesis of new metalla-architectures, evidence for the potential of using these electron-rich metalla-assemblies to

Received: December 16, 2013
Published: March 27, 2014

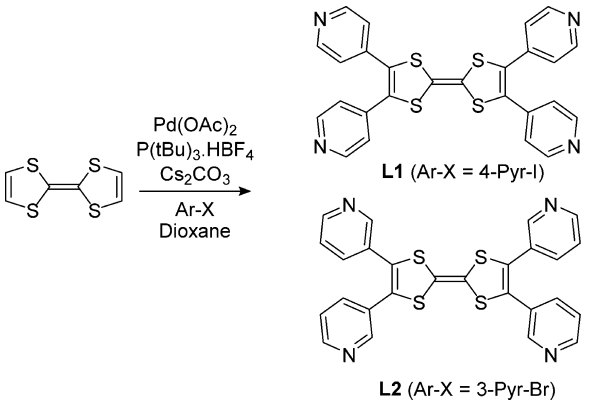
 © 2014 American Chemical Society dx.doi.org/10.1021/om401142j | *Organometallics* 2014, 33, 1651–1658

interact with planar electron-deficient molecules was demonstrated by X-ray diffraction studies.

RESULTS AND DISCUSSION

Synthesis and Characterization of the Tetratopic Ligands L1 and L2. The ligand **L1**, unknown so far, was prepared by an adaptation of the reported synthesis procedure for **L2**.[11] The reaction of halo-pyridine (4-iodopyridine for **L1** and 3-bromopyridine for **L2**) with tetrathiafulvalene in the presence of $Pd(OAc)_2$, tri-*tert*-butylphosphine tetrafluoroborate, and Cs_2CO_3 in refluxing dioxane yielded the desired ligands in good yield (Scheme 1).

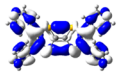
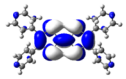
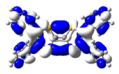
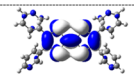
Scheme 1. Synthesis of Ligands L1 and L2



X-ray Structure of L1. Single crystals of **L1**, which deteriorate rapidly, were obtained by slow diffusion of hexane in a dichloromethane solution of **L1**. In the crystal packing, the pyridyl groups are rotated along the TTF−Py axis by values ranging from 31° to 77° (Figure 1a). Similar distortions were found with a tetrapyridyl(vinylenedithio) TTF derivative in the solid state.[12] The four N_{pyr} atoms of **L1** define a rectangle of approximately 6.7 Å × 13.1 Å^2. An angle of 73° is found between vicinal pyridine axes. Such geometric data are important to consider in order to address the subsequent self-assembly processes, and additional computational studies were carried out to answer this issue.

Theoretical Calculations of Ligands L1 and L2. In order to anticipate the electronic and geometrical behaviors of ligands **L1** and **L2**, theoretical calculations based on density functional theory (DFT) methods were performed with the Gaussian 09 program.[13] Becke's three-parameter gradient-corrected functional (B3LYP) with 6-31G(d,p) basis in vacuo was used for full geometry optimization and to compute the electronic structure at the minima found. The resulting frontier molecular orbitals are shown in Table 1. A first striking observation comes

Table 1. Frontier Molecular Orbitals of Ligands L1 and L2 (DFT, B3LYP, 6-31G(d,p))

	LUMO	HOMO
L1		
L2		

from the fact that both optimized geometries of ligands **L1** and **L2** reveal a significant rotation of the pyridyl groups around the TTF−Py bond by 44−49° (Figure 1b). This result strongly differs from the case of the BPTTF tetrapyridyl ligand,[8a] for which the four electron-withdrawing pyridyl units were conjugated to the coplanar central BPTTF unit, resulting in an alteration of its π-donating ability. Contrariwise, in the case of **L1** and **L2**, the pyridyl groups cannot be in the TTF plane because of the steric contraction brought by their vicinal positions. Therefore, in **L1** and **L2**, the latter should not contribute to decrease drastically the π-donating ability of TTF through conjugation, thus preserving the intrinsic electronic properties of the redox moiety. This is confirmed by the energy values of the HOMO orbitals (**L1**: −5.11 eV; **L2**: −4.86 eV), lower than for the parent TTF (−4.52 eV), but still reflecting a good π-donating ability. It is clear from these calculations that the electron density of the HOMO orbital is located on the TTF fragment (see Table 1), while the LUMO is essentially distributed over the whole molecule including the pyridyl groups.

Electronic Properties of Ligands L1 and L2. UV−visible spectra of **L1** and **L2** exhibit two absorption bands at λ < 350 nm (Figure S22), which are assigned to the local transition in the TTF moiety. A third broader absorption at a lower energy and centered at 450 nm is attributed to an intramolecular charge transfer between the donating unit and the electron-withdrawing pyridyl groups.[14] The experimental HOMO−LUMO gap measured from these spectra is in good accordance with the theoretical values obtained from DFT calculations (Table S1).

The electrochemical properties of **L1** and **L2** were further investigated by cyclic voltammetry (1:1 CH_2Cl_2/CH_3CN, NBu_4PF_6) (Figure S21). Two reversible oxidation waves are observed, located at higher potentials than those of the parent TTF system (**L1**: E^1_{ox}= 0.22 V, E^2_{ox}= 0.55 V; **L2**: E^1_{ox} = 0.12 V, E^2_{ox} = 0.47 V vs Fc/Fc^+), in accordance with the electron-accepting character of the pyridyl groups and as anticipated from the corresponding HOMO values. The difference in E_{ox} values between **L1** and **L2** is in full agreement with the

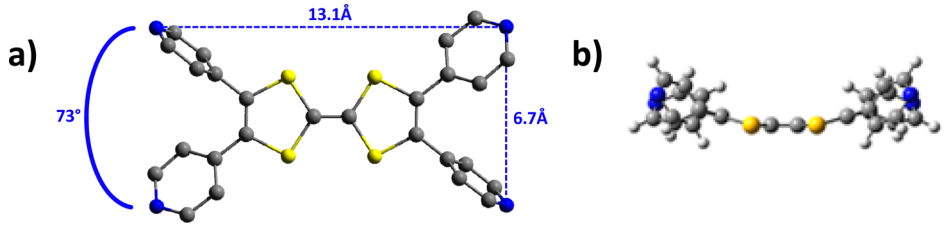
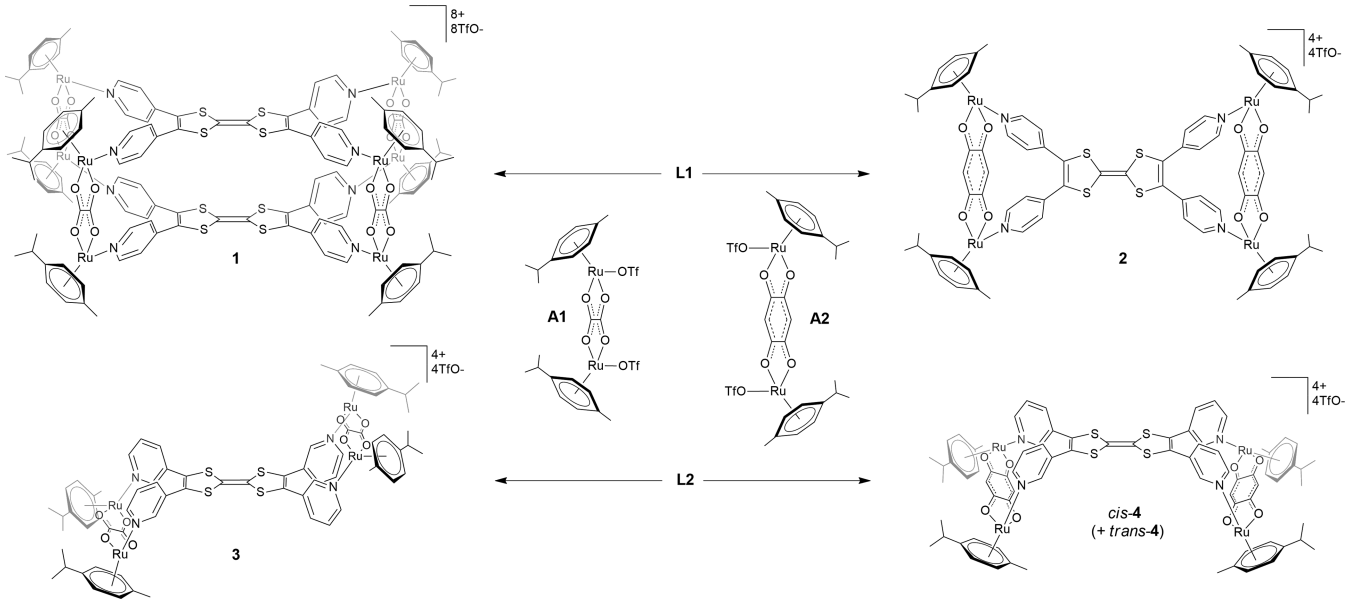


Figure 1. Ball-and-stick views of **L1**, showing the main geometrical parameters: (a) top view (X-ray structure); (b) side view (Geometric optimization).

dx.doi.org/10.1021/om401142j | *Organometallics* 2014, 33, 1651−1658

Scheme 2. Synthesis of Redox-Active Metalla-assemblies 1−4



respective electronic effects generated by the N-pyridyl atom in the 4- versus 3-positions.[15]

Synthesis and Characterizations of Metalla-architectures 1−4. The reaction of **L1** with arene−ruthenium acceptor **A1** in a 1:2 molar ratio in methanol affords the discrete octanuclear [2+4] cube **1** after stirring for 12 h at room temperature, whereas the tetranuclear [1+2] plate **2** is obtained by the reaction (12 h) of a 1:2 mixture of **L1** with the arene−ruthenium acceptor **A2** in methanol (Scheme 2). The formation of two different architectures by varying only the length of the acceptor can be explained by self-sorting of proper geometric complementary interactions. As stated above from the X-ray single-crystal structure analysis of **L1**, two nitrogen atoms belonging to two adjacent pyridyl groups in ligand **L1** are separated by 6.7 Å. On the other hand, the distance between two Ru atoms in **A1** is approximately 5.5 Å,[2c] and the metal−metal distance reaches a value of 7.9 Å in the case of **A2**.[2d] Therefore, whereas a perfect size matching is observed between **L1** and the dimetallic complex **A2**, thus favoring formation of the tetranuclear plate structure **2**, an octanuclear cage **1** is observed from the smaller diruthenium acceptor **A1**. Cube **1** was isolated by precipitation with diethyl ether and characterized by ^{1}H NMR spectroscopy in methanol-d_4 (Figure S5). In addition to the expected metal-coordination-induced upfield shift of the H_{pyr} resonances as compared to **L1**, additional splitting of the pyridyl protons is observed (2:1:1 at δ = 8.13, 7.46, and 7.09 ppm), suggesting a restricted rotation of the pyridyl groups upon formation of the metallacubes. Such splitting of the pyridyl signals is assigned to the steric interaction between adjacent coordinated pyridyl groups.[9a] On the other hand, two doublets at δ = 8.10 ppm (H_α) and 7.45 ppm (H_β) are observed in methanol-d_4 for the pyridyl protons of metallaplate **2** (Figure S8). ^{1}H diffusion-ordered spectroscopy (DOSY) NMR spectra of **1** and **2** show the presence of a single alignment of the signals for both metalla-assemblies, confirming the formation of one discrete species in both cases. The diffusion coefficients extracted from the DOSY experiments of **1** ($D \approx 2.14 \times 10^{-10}$ m^2 s^{-1}) and **2** ($D \approx 3.43 \times 10^{-10}$ m^2 s^{-1}) are significantly different and suggest two distinctive structures with respective hydrodynamic radii of 18.5 and 11.5 Å calculated from the Stokes−Einstein equation (T = 298 K).[16]

The high-resolution ESI-MS data confirm the formation of the [2+4] octanuclear cube **1** and the [1+2] tetranuclear plate **2**. Peaks attributed to the consecutive loss of triflate counterions $[\mathbf{1} - 2CF_3SO_3]^{2+}$, m/z 2078.88, $[\mathbf{1} - 3CF_3SO_3]^{3+}$, m/z 1336.28 for **1** and $[\mathbf{2} - 3CF_3SO_3]^{3+}$, m/z 1014.99, $[\mathbf{2} - 3CF_3SO_3]^{3+}$, m/z 627.01 for **2** are observed. Experimental isotopic patterns perfectly correlate with the calculated theoretical isotopic distributions (Figures S17 and S18) and attest to the different nuclearities of the systems. Unfortunately, all attempts to grow diffraction quality crystals of **1** and **2** have failed so far in our hands.

As anticipated from the coordination angles promoted by ligand **L2** as compared to **L1**, quite different structures are found upon metal-driven self-assembly. Using the same experimental conditions as for **L1**, only [1+2] metalla-assemblies were obtained from **L2** with both **A1** and **A2** acceptors (Scheme 2). The reaction of **L2** with **A1** leads to the exclusive formation of [1+2] *trans*-metalla-assembly **3**, whereas the reaction with **A2** affords a mixture of *cis*-**4** and *trans*-**4** isomeric metallaplates in a 1:1 ratio. The ^{1}H NMR spectra of **3** and **4** show characteristic resonances for the pyridyl protons with significant metal-coordination-induced upfield shifts as compared to free ligand **L2**. The formation of a *cis/trans* mixture in the case of **4** is supported by the presence of two sets of signals for the *p*-cymene units in the ^{1}H NMR spectrum. Similar diffusion coefficients ($D \approx 3.48 \times 10^{-10}$ m^2 s^{-1}) are extracted from the DOSY NMR spectra of **3** and **4** (Figures S13 and S16), which supports the occurrence of structurally similar metalla-assemblies in each case. Further ESI-MS analysis confirmed the formation of [1+2] self-assembled tetranuclear metalla-assemblies **3** and **4** by the appearance of multiply charged fragmented ions. Peaks at m/z = 964.97 $[\mathbf{3} - 2CF_3SO_3]^{2+}$, 593.66 $[\mathbf{3} - 3CF_3SO_3]^{3+}$, 408.01 $[\mathbf{3} - 4CF_3SO_3]^{4+}$ and at m/z = 1014.99 $[\mathbf{4} - 2CF_3SO_3]^{2+}$, 627.01 $[\mathbf{4} - 3CF_3SO_3]^{3+}$ were observed. Their well-resolved isotopic patterns strongly support the formation of [1+2] metalla-assemblies in both cases (Figures S19 and S20).

dx.doi.org/10.1021/om401142j | *Organometallics* 2014, 33, 1651−1658

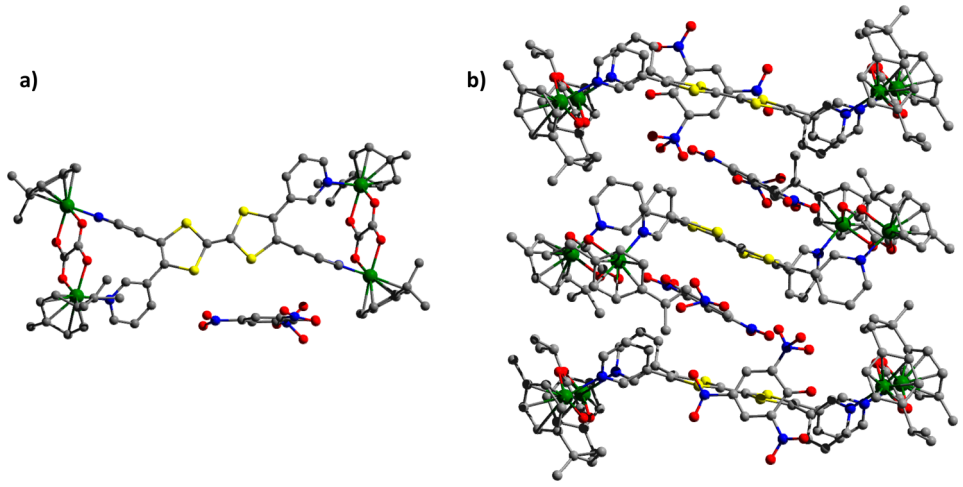


Figure 2. X-ray structure of **3**·PA (a) and packing diagram (b). Solvent molecules and hydrogen atoms are omitted for clarity (color codes: S = yellow, Ru = green, O = red, N = blue, and C = gray).

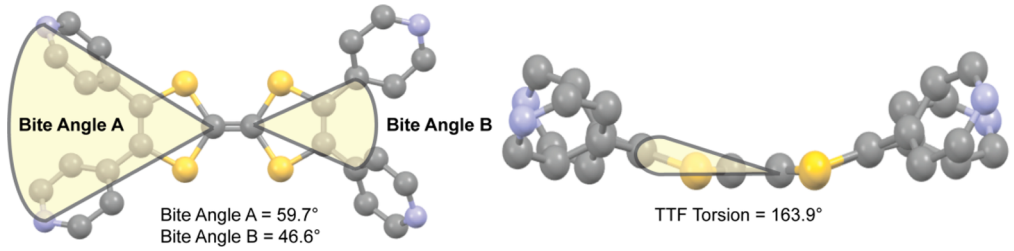


Figure 3. DFT-optimized geometry of free ligand **L1** illustrating important angles and torsion angles used for the analysis of metalla-assemblies.

The molecular structures of **3**, *cis*-**4**, and *trans*-**4** as proposed by the NMR spectroscopy were unambiguously confirmed by single-crystal X-ray structure analyses. Although we were unable to get single crystals for the discrete metalla-assemblies, we could circumvent this difficulty by performing cocrystallization with an aromatic organic molecule. Indeed, considering the electron-rich character of the TTF-based metalla-assemblies in **3** and **4**, we explored their ability to interact with electron-deficient derivatives. Two equivalents of picric acid (PA) in methanol were therefore layered on a CH_2Cl_2 solution of **3**, and crystals of the picric acid complex **3**·PA were grown by slow diffusion of pentane. Single-crystal X-ray structure analysis of **3**·PA reveals that **3** is present in a *trans* configuration (assigned on the relative spatial position of the bimetallic parts related to the TTF plane). The two ruthenium centers from one acceptor moiety are separated by 5.521(1) Å, and the average Ru−N and Ru−O bond distances are 2.153(6) and 2.121(6) Å, respectively (Figure 2a).

The driving force behind the selective formation of the *trans* isomer is likely the strain that is associated with the *cis* isomer, which is alleviated in the *trans* derivative. The solid-state packing diagram of **3** results in a stacked structure involving $\pi-\pi$ interactions between the TTF moiety and the PA unit (Figure 2b) with interplanar distances of 3.4−3.6 Å. Interestingly, both isomers of **4** crystallize as their PA complexes, *cis*-**4**·PA and *trans*-**4**·PA, respectively, by slow diffusion of pentane on a solution of picric acid (2 equiv) in methanol layered on a CH_2Cl_2 solution of **4**. Although poorly resolved because of the low quality of the crystals, the X-ray diffraction study on *cis*-**4**·PA shows that four picric acid molecules are trapped between two *cis*-**4** units (Figure S23).

In the *cis*-**4** isomer, the four N-py atoms of **L2** are rotated toward the same face of the TTF plane. Consequently, the four ruthenium atoms form a rectangle (7.84 Å × 9.46 Å) that is parallel to the TTF plane (Figure S23). In the case of *trans*-**4**·PA (Figure S23), one Ru-acceptor moiety lies on each side of the TTF skeleton, and a completely different stacking mode is observed, with interplanar distances of ∼3.53−3.99 Å between the planes of the picric acid and the TTF moiety, a standard value for $\pi-\pi$ stacking interactions.

DFT Calculations on Metalla-architectures 1−4. In order to have a better understanding on the structural characteristics of the newly designed metalla-assemblies, further DFT studies were undertaken. Computational models of the ruthenium coordination complexes were composed of the complete experimental ligand sphere (i.e., **A1** or **A2** and **L1** or **L2**) with the exception of the replacement of the *p*-cymene with a benzene ring. The metrical parameters obtained from X-ray structure determinations of the tetracationic metalla-assemblies **3** and **4** were used to consider the geometric accuracy of a selection of DFT functionals and basis sets (see the Supporting Information). The PBE0 functional, designated PBE1PBE in Gaussian, was chosen for subsequent full gas-phase geometry optimization calculations.

Three geometrical parameters related to the TTF ligand, as defined in Figure 3, proved to be useful in the subsequent structural analysis of the metalla-assemblies. The bite angle **A** is composed by the 4-position of the pyridine rings (i.e., N or C for **L1** and **L2**, respectively) and the central disulfur-substituted sp^2-carbon. The bite angle **B** corresponds to the same central disulfur-substituted sp^2-carbon and the position-1 of the pyridine rings. These two angles are sensitive to the geometric constraints conferred by different diruthenium acceptor

dx.doi.org/10.1021/om401142j | *Organometallics* 2014, 33, 1651−1658

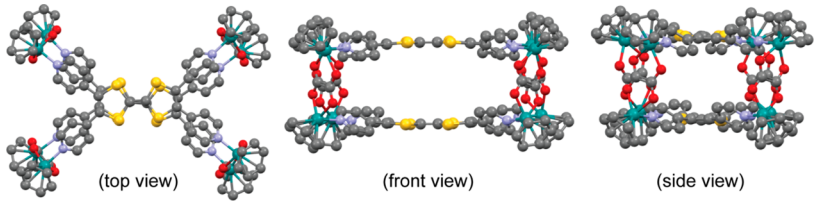


Figure 4. DFT-optimized geometry of the octacationic cube **1**. Hydrogen atoms have been removed for clarity (color codes: Ru = aquamarine, O = red, N = blue, C = gray).

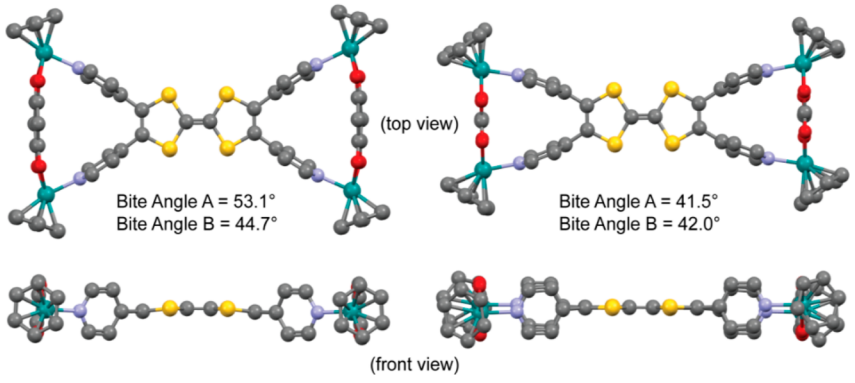


Figure 5. DFT-optimized geometry of the tetracationic metallaplate **2** (**A2** + **L1**) (left) and the hypothetical planar complex (**A1** + **L1**) (right). Hydrogen atoms have been removed for clarity (color codes: Ru = aquamarine, O = red, N = blue, C = gray).

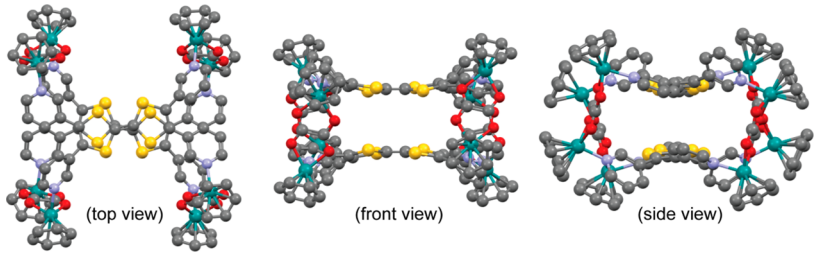


Figure 6. DFT-optimized geometry of the hypothetical octacationic metallacube with acceptor **A1** and donor **L2**. Hydrogen atoms have been removed for clarity (color codes: Ru = aquamarine, O = red, N = blue, C = gray).

scaffolds. The torsional angle of the TTF ring system also proved to be useful.

Geometry optimization of metallacage **1** yielded a stationary point (Figure 4). The number of atoms made the normal-mode analysis computationally inaccessible. Nevertheless, the optimized structure exceeded the default Gaussian convergence criteria and had a predicted energy change of 0.001 kcal/mol. We are therefore confident that the identified structure represents a realistic model for cube **1**.

As anticipated, the structural parameters of the cube are quite similar to those of the corresponding free species. Diruthenium acceptor **A1**, constituting the sides of the metalla-assembly, does not show any perturbation in length from the free species (i.e., 5.5 Å). The donor TTF moieties (**L1**), constituting the floor and ceiling of the cube, show a slight relaxation of the bite angles A and B (62.0° and 47.4°, respectively) and a nearly planar TTF torsion angle of 176.5°. The torsion of the pyridyl rings relative to the TTF plane is 41.2° and 36.1°, respectively. The donor TTF planes are separated by 6.3 Å, and the volume of the cavity, based on the ruthenium centers, is estimated to be 870 Å^3.

Geometry optimization calculations were also performed on metallaplate **2** (**A2** + **L1**) and the experimentally unobserved plate complex resulting from coordination between acceptor **A1** and **L1** (Figure 5). Consistent with the expectation, the TTF ligand of plate **2** is structurally similar to the free TTF ligand **L1**. The distance between the pyridine rings has slightly contracted to accommodate acceptor **A2** (bite angle A = 53.1°), and the TTF ring has moved closer to planarity (TTF torsion = 174.5°).

Accordingly, the hypothetical metallaplate involving acceptor **A1** and **L1** shows a significant contraction of the distance between the pyridyl rings (bite angle A = 41.5°). The increased strain from this contraction is estimated to cost nearly 8 kcal/mol in enthalpy. This energetic cost is likely the most important factor in determining the selectively for the cube versus the plate for a given combination of donor/acceptor moieties (Figures 5 and 6).

We were also interested in understanding why the reaction between the acceptor **A1** and the donor **L2** yielded the tetranuclear metallaplate **3**, rather than a metallacube similar to **1**. Geometry optimization of the hypothetical cube (**A1** + **L2**) was performed, and a stationary point was identified (Figure 6). There are two notable features of this cube. First, the TTF torsion angle is 170° with the acceptor moieties sitting on the convex face of the ligand. The fact that the tetranuclear *cis*-metallaplate **3** is not observed suggests that this conformation leads to an energetic penalty. Second, the acceptor moieties

dx.doi.org/10.1021/om401142j | *Organometallics* 2014, 33, 1651−1658

have shifted from the vertices to the sides of the cube. This structural change results in a significant contraction of two pyridyl torsional angles (32° and 33°), while the other two angles slightly relaxed (47° and 48°) relative to **L2** (44.9° and 46.6°). Taking these features together, it appears that significant structural strain is generated in this cubic hypothetical molecule. The strain is not manifested in the free TTF ligand though. The compositional isomers **L1** and **L2** are nearly isoenergetic (**L1** is less stable by −0.5 kcal/mol). However, the comparison of the total energy of metallacube **1** (**A1** + **L1**) and the hypothetical one (**A1** + **L2**) shows that the latter is less stable by 46 kcal/mol, indicating that its formation is highly unfavorable.

The tetranuclear complexes obtained with 3-pyridyl-TTF donor **L2** were also considered. We sought to rationalize why selective formation of a *trans* isomer was observed with **A1** (metallaplate **3**), while a 1:1 mixture of *cis* and *trans* tetranuclear metalla-assemblies was observed with **A2** (metalla-assemblies **4**) (Tables S3−5). The latter isomers (**A2** + **L2**) yielded a gas-phase relative enthalpy and free energy of less than 0.5 kcal/mol, which was anticipated based on the experimental results. The metrical parameters of the isomers are also quite similar, with the exception of the TTF torsion (162° and 176° for *cis*-**4** and *trans*-**4**, respectively). When the former isomers (**A1** + **L2**) were compared, we were surprised to find a similar energetic result: the isomers were isoenergetic in terms of both relative enthalpy and free energy (ΔH = 0.13 and ΔG = 0.14 kcal/mol). The metrical parameters of metallaplate **3** show only small perturbations from those of **4**. Bite angles A and B contract slightly with the smaller acceptor (5° and 1°, respectively). The acceptor length is largely accommodated by changes to the pyridyl ring torsion relative to the TTF backbone. Both isomers of **3** have torsions that are 4° from orthogonal, while both isomers of **4** have torsions that are 15° from orthogonal. The structural similarities and differences in the **L2** structure for the tetranuclear metalla-assemblies led us to assess the conformational flexibility of **L2** by performing single-point energy calculations on the isolated **L2** ligand geometries from the four optimized metalla-architectures. Even though large torsional differences exist in the structures, the relative energies remain quite similar across all four structures (ΔE < 0.5 kcal/mol).

Observed DFT calculations suggest, and experimental data confirm, that the tetranuclear ruthenium complexes are kinetically nonlabile, so we reasoned that selectivity for the *trans* isomer could result from the energetic differentiation of the dinuclear intermediates (1 + 1 equiv of **A1** + **L2**). Geometry optimization calculations were performed for two conformations of the dinuclear intermediate with the free pyridyl ligands oriented such that they could yield the corresponding tetranuclear isomers. The predicted relative enthalpy and free energy changes were again quite small (<0.2 kcal/mol). Our computational studies have not allowed us to rationalize the selectivity for *trans*-**3**. The error associated with the local minima energies by DFT (±3 kcal/mol) may provide the most logical explanation; however, an as yet unidentified and unexplained noncovalent interaction present during the reaction (**A1** + **L2**) also cannot be ruled out.

Electronic Properties of Metalla-architectures 1−4. The UV−visible spectroscopic properties of **1**−**4** (1×10^{-5} M) were investigated in methanol (Figure S22). The electronic spectra show peaks at λ = 274 and 379 nm for **1**, λ = 278 and 493 nm for **2**, λ = 271 and 378 nm for **3**, and λ = 285 and 493 nm for **4**. These bands are likely due to the combination of intra/intermolecular $\pi \rightarrow \pi^*$ mixed with metal-to-ligand charge transitions.

Cyclic voltammetry (CV) studies of **1**−**4** (5×10^{-4} M) were performed in CH_3CN containing 0.1 M n-Bu_4NPF_6 as supporting electrolyte (Figure 7). Metalla-assemblies **2**−**4** exhibit the usual two successive one-electron reversible oxidation behavior that is typical of TTF derivatives (**2**: E^1_{ox} = 0.28 V, E^2_{ox} = 0.58 V; **3**: E^1_{ox} = 0.34 V, E^2_{ox} = 0.66 V; **4**: E^1_{ox} = 0.23 V, E^2_{ox} = 0.52 V vs Fc/Fc^+). These values appear at slightly higher potentials than for their parent ligands **L1** and **L2**, as anticipated from coordination of the pyridyl groups to metal centers. The three compounds exhibit a similar ΔE value ($E^2_{ox} - E^1_{ox}$) of 0.29−0.32 V and present only small differences in their respective π-donating ability (E^1_{ox}), which presumably accounts for the combined electronic effect generated by the accepting moiety (**A1** vs **A2**) and the TTF ligand (**L1** vs **L2**). One can notice that metalla-assembly **4** exhibits a better π-donating ability than **3** (lower E_{ox} values), synthesized from the same ligand **L2**. This observation is ascribed to the higher delocalization in acceptor **A2** than in **A1**, leading to a lower electron-withdrawing effect. Nevertheless, in all of these cases the metalla-assemblies present a high π-donating ability ascribed to the TTF contribution.

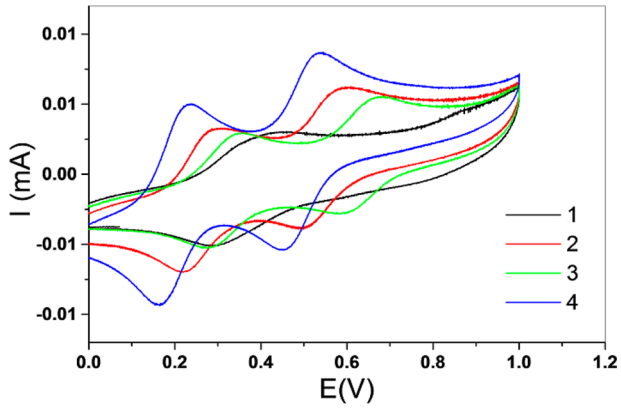


Figure 7. Cyclic voltammograms of metalla-assemblies **1**−**4** ($c = 5 \times 10^{-4}$ M, CH_3CN, 0.1 M NBu_4PF_6, 50 mV s^{-1}, Pt, V vs Fc/Fc^+).

Consistent with the different molecular formulation of **1** as compared to **2**−**4**, the electrochemical behavior observed for metallacube **1** is significantly different. A single oxidation wave is observed for **1**, located in the usual oxidation potentials range of TTF derivatives (E^1_{ox} = 0.44 V). Such nonclassical electrochemical behavior, regarding TTF derivatives, was already observed in the case of a three-dimensional self-assembled architecture.[6a] This peculiar behavior is ascribed to the rigidity of the metal-assembled cube, which may alter the kinetics of the conformational changes that accompany the electrochemical processes.

CONCLUSIONS

Compounds **L1** and **L2** are of great interest regarding their dual redox and coordinating properties. The X-ray structure analysis of ligand **L1** has provided and illustrated the potential of this new ligand for the construction of metalla-assemblies with redox-active architectures. On this ground, a set of TTF-based metalla-assemblies have been prepared from two isomeric tetrapyridyl-TTF ligands **L1** and **L2** and two dinuclear arene

dx.doi.org/10.1021/om401142j | *Organometallics* 2014, 33, 1651−1658

ruthenium acceptors. Computational studies have supported the formation of the different self-assembled architectures from the various combinations between those species. A TTF-based redox-active cubic metalla-assembly has been described for the first time. This result opens promising perspectives in terms of new electron-rich three-dimensional assemblies designed for guest transport properties or catalytic purposes. All new redox-active assemblies were characterized by ^{1}H, ^{13}C, and DOSY-NMR spectroscopy and HR-ESI-MS. A first illustration of these electron-rich assemblies to associate electron-deficient species was provided with picric acid and complexes **3**, *cis*-**4**, and *trans*-**4**, which showed, by single-crystal X-ray structure analyses, cocrystalline products.

EXPERIMENTAL DATA

General Details. Arene−ruthenium acceptors (**A1**[2c] and **A2**[2d]) were prepared according to reported methods. Deuterated solvents were purchased from Cambridge Isotope Laboratory (Andover, MA, USA). NMR spectra were recorded on a NMR Bruker Avance III 300 spectrometer. ^{1}H NMR chemical shifts were reported relative to residual solvent signals. MALDI-TOF-MS spectra were recorded on a MALDI-TOF Bruker Bifle III instrument using a positive-ion mode. ESI-MS spectra were achieved on a Bruker MicrO-Tof-Q 2 spectrometer in CH_2Cl_2. Cyclic voltammetry experiments were carried out on ALS electrochemical analyzer model 660, with the following conditions: 0.1 M n-Bu_4NPF_6 in distilled acetonitrile, Ag/Ag^+ reference electrode, C-graphite working electrode, and Pt counter electrode, 50 mV s^{-1}, calibrated using internal ferrocene. UV/visible/NIR absorption spectra were recorded on a PerkinElmer Lamda19 spectrometer, and spectroscopic grade solvents were used.

Single-Crystal X-ray Crystallography. X-ray single-crystal diffraction data were collected at different low temperatures on a Bruker KappaCCD diffractometer, equipped with a graphite monochromator utilizing Mo Kα radiation (λ = 0.71073 Å). The four structures were solved by direct methods, expanded using difference Fourier map for **3**·PA, *cis*-**4**·PA, and *trans*-**4**·PA and refined on F^2 by full matrix least-squares techniques using the SHELX97 (G. M. Sheldrick, 1998) package. For all structures, all non-hydrogen atoms were refined anisotropically, except for *cis*-**4**·PA, where C atoms were refined isotropically. Absorption was corrected by the SADABS program (Sheldrick, Bruker, 2008). The H atoms were found by Fourier difference map for **L1**, and they were included in the calculation without refinement for **3**·PA. No H atoms were added for *cis*-**4**·PA and *trans*-**4**·PA because of nonconvergent refinement.

General Procedure for the Synthesis of Ligands L1 and L2. To a suspension of palladium acetate (82 mg, 0.36 mmol), tri-*tert*-butylphosphine tetrafluoroborate (320 mg, 1.10 mmol), and cesium carbonate (2.40 g, 7.30 mmol) stirred for 10 min at 90 °C under argon in distilled dioxane (20 mL) was added an argon-degassed solution of tetrathiafulvalene (300 mg, 1.46 mmol) and the halogenated pyridine [4-iodopyridine (for **L1**) and 3-bromopyridine (for **L2**)] in dioxane (20 mL). The reaction was stirred under reflux for 24 h. After cooling, a large excess of dichloromethane and water were added. The aqueous phase was extracted, and the organic extracts were washed with brine, dried over magnesium sulfate, filtered, and concentrated. The residue was purified by chromatography on silica gel (deactivated with triethylamine 1%).

Ligand ***L1***. This was prepared following experimental conditions as discussed above: from 4-iodopyridine (1.50 g, 7.34 mmol); chromatography eluting from dichloromethane to dichloromethane/methanol (97:3 v/v) to give a red powder (530 mg, 1.03 mmol, 71%). Crystals (dark red needles) were obtained by slow diffusion of hexanes in dichloromethane. Melting point: >260 °C. ^{1}H NMR [300 MHz, $CDCl_3$]: δ (ppm) 8.55 (d, ^{3}J = 6.2 Hz, 4H, Hα), 7.09 (d, ^{3}J = 6.2 Hz, 4H, Hβ). ^{13}C NMR [75 MHz, $CDCl_3$]: δ (ppm) 150.6, 139.4, 129.5, 123.1, 108.9. MS (MALDI-TOF) for [$C_{26}H_{16}N_4S_4$]: calculated 512.69; observed 512.5. Anal. Calcd for $C_{26}H_{16}N_4S_4$: C, 60.91; H, 3.15; N, 10.93; S, 25.02. Found: C, 60.70; H, 3.15; N, 10.79, S, 24.94.

Ligand ***L2*** *(ref 11)*. This was prepared by following experimental conditions discussed above: from 3-bromopyridine (1.20 g, 7.34 mmol); chromatography eluting from dichloromethane to dichloromethane/methanol (97:3 v/v) to give a dark red powder (449 mg, 0.88 mmol, 60%). Melting point: >260 °C. ^{1}H NMR [300 MHz, $CDCl_3$]: δ (ppm) δ 8.56 (d, ^{3}J = 3.8 Hz, 4H, Hα), 8.49 (d, ^{3}J = 3.8 Hz, 4H, Hβ), 7.57 (m, 4H, Hγ), 7.25 (m, 4H, Hα'). ^{13}C NMR [75 MHz, $CDCl_3$]: δ (ppm) 149.8, 149.6, 136.3, 128.2, 127.7, 123.5, 108.9. MS (MALDI-TOF) for $C_{26}H_{16}N_4S_4$: calculated 512.69; observed 512.5.

General Procedure for the Synthesis of Metalla-assemblies 1−4. A solution of methanol (2 mL) was added to a solid sample of the corresponding arene−ruthenium acceptor (**A1** and **A2**) and TTF-based donor (**L1** or **L2**) in 2:1 molar ratio. The mixture was stirred at room temperature for 12 h, after which the solution was concentrated and diethyl ether added to precipitate the pure self-assembled metallacycles.

Metalla-assembly ***1***. Acceptor clip **A1** (8.56 mg, 0.01 mmol) and tetrapyridyl donor **L1** (2.56 mg, 0.005 mmol) were stirred in methanol (2 mL) to obtain **1** as a brown solid, which was isolated by precipitation with Et_2O. Isolated yield: 81%. ^{1}H NMR [300 MHz, CD_3OD]: δ (ppm) 8.13 (br d, ^{3}J = 6.0 Hz, 16H, Hα), 7.46 (d, ^{3}J, H = 6.0 Hz, 8H, Hβ), 7.09 (m, 8H, Hβ), 6.08−5.77 (m, 32H, Hcym), 2.86 (m, 8H, C*H*(CH_3)$_2$), 2.28 (m, 24, CH_3), 1.38 (m, 48H, CH(C*H*$_3$)$_2$). ^{13}C NMR (75 MHz, CD_3OD): δ (ppm) 170.5, 153.1, 141.8, 140.5, 130.6, 125.8, 124.6, 122.6, 118.4, 102.0, 101.5, 98.2, 97.5, 83.5, 82.7, 82.3, 81.8, 81.7, 31.0, 21.3, 21.1, 16.9, 16.7. HRMS (ESI) for $C_{148}H_{144}F_{24}N_8O_{40}Ru_8S_{16}$: calculated 2076.9007 [**1** − 2OTf]$^{2+}$, 1335.2829 [**1** − 3OTf]$^{3+}$; observed 2076.8788 [**1** − 2OTf]$^{2+}$, 1335.2830 [**1** − 3OTf]$^{3+}$. Anal. Calcd for $C_{148}H_{144}F_{24}N_8O_{40}Ru_8S_{16}$: C, 39.93; H, 3.26; N, 2.52. Found: C, 39.78; H, 2.99; N, 2.34.

Metalla-assembly ***2***. Acceptor clip **A2** (9.06 mg, 0.01 mmol) and tetrapyridyl donor **L1** (2.56 mg, 0.005 mmol) were stirred in methanol (2 mL) to obtain **2** as a dark red solid, which was isolated by precipitation with Et_2O. Isolated yield: 85%. ^{1}H NMR [300 MHz, CD_3OD]: δ (ppm) 8.14 (d, ^{3}J = 6.0 Hz, 8H, Hα), 7.41 (d, ^{3}J = 6.0 Hz, 8H, Hβ), 6.09 (d, 8H, ^{3}J = 6.0 Hz, Hcym), 5.87 (d, 8H, ^{3}J = 6.0 Hz, Hcym), 5.63 (s, 4H, Hbq), 2.91 (m, 4H, C*H*(CH_3)$_2$), 2.27 (s, 12H, CH_3), 1.37 (d, ^{3}J = 6.0 Hz, 24H, CH(C*H*$_3$)$_2$). ^{13}C NMR (75 MHz, CD_3OD): δ (ppm) 184.4, 154.8, 144.5, 130.1, 128.6, 123.1, 120.6, 111.6, 105.3, 102.9, 99.9, 84.6, 83.3, 32.6, 22.6, 18.3. HRMS (ESI) for $C_{82}H_{76}F_{12}N_4O_{20}Ru_4S_8$: calculated 1014.4897 [**2** − 2OTf]$^{2+}$, 626.6766 [**2** − 3OTf]$^{3+}$; observed 1014.4880 [**2** − 2OTf]$^{2+}$, 626.6757 [**2** − 3OTf]$^{3+}$. Anal. Calcd for $C_{82}H_{76}F_{12}N_4O_{20}Ru_4S_8$: C, 42.34; H, 3.29; N, 2.41. Found: C, 41.96; H, 3.04; N, 2.26.

Metalla-assembly ***3***. Acceptor clip **A1** (8.56 mg, 0.01 mmol) and tetrapyridyl donor **L2** (2.56 mg, 0.005 mmol) were stirred in methanol (2 mL) to obtain **3** as a brown-yellow solid, which was isolated by precipitation with Et_2O. Isolated yield: 84%. ^{1}H NMR [300 MHz, CD_3OD]: δ (ppm) 8.90 (d, ^{3}J = 6.0 Hz, 4H, Hα), 7.92 (d, ^{3}J = 6.0 Hz, 4H, Hβ), 7.50 (s, 4H, Hα'), 7.46 (d, ^{3}J = 6.0 Hz, 4H, Hγ), 6.05 (d, ^{3}J = 6.0 Hz, 8H, Hcym), 5.87 (d, ^{3}J = 6.0 Hz, 8H, Hcym), 2.87 (m, 4H, C*H*(CH_3)$_2$), 2.28 (s, 12H, CH_3), 1.36 (d, ^{3}J = 6.0 Hz, 24H, CH(C*H*$_3$)$_2$). ^{13}C NMR (75 MHz, CD_3OD): δ (ppm) 157.2, 151.0, 143.3, 131.8, 130.3, 128.0, 124.0, 119.8, 111.2, 102.7, 99.6, 82.9, 32.5, 22.5, 18.2. HRMS (ESI) for $C_{74}H_{72}F_{12}N_4O_{20}Ru_4S_8$: calculated 963.9740 [**3** − 2OTf]$^{2+}$, 592.9965 [**3** − 3OTf]$^{3+}$, 407.5108 [**3** − 4OTf]$^{4+}$; observed 963.9702 [**3** − 2OTf]$^{2+}$, 592.9965 [**3** − 3OTf]$^{3+}$, 407.5098 [**3** − 4OTf]$^{4+}$. Anal. Calcd for $C_{74}H_{72}F_{12}N_4O_{20}Ru_4S_8$: C, 39.93; H, 3.26; N, 2.52. Found: C, 40.29; H, 2.89; N, 2.18.

Metalla-assembly ***4***. Acceptor clip **A2** (9.06 mg, 0.01 mmol) and tetrapyridyl donor **L2** (2.56 mg, 0.005 mmol) were stirred in methanol (2 mL) to obtain **4** as a dark red solid, which was isolated by precipitation with Et_2O. Isolated yield: 82%. ^{1}H NMR [300 MHz, CD_3OD]: δ (ppm) 8.83 (d, ^{3}J = 6.0 Hz, 4H, Hα), 8.17 (d, ^{3}J = 6.0 Hz, 4H, Hγ), 7.52 (m, 4H, Hβ), 7.42 (s, 2H, Hα'), 7.37 (s, 2H, Hα'), 6.30 (s, 2H, Hbq), 6.21−5.85 (m, 16H, Hcym), 5.29 (d, 2H, ^{3}J = 6.0 Hz, Hbq), 2.92 (m, 4H, C*H*(CH_3)$_2$), 2.32 (s, 6H, CH_3), 2.29 (s, 6H, CH_3), 1.37 (m, 24H, CH(C*H*$_3$)$_2$). ^{13}C NMR (75 MHz, CD_3OD): δ (ppm) 185.24, 185.22, 184.09, 184.05, 157.3, 151.7, 151.4, 143.4, 130.9, 129.6, 129.5, 127.6, 127.5, 123.1, 120.6, 110.8, 110.4, 104.4,

dx.doi.org/10.1021/om401142j | *Organometallics* 2014, 33, 1651−1658

104.3, 104.1, 102.3, 100.9, 99.2, 85.8, 85.7, 83.4, 82.9, 82.7, 82.0, 81.2, 32.68, 32.65, 23.0, 22.9, 22.5, 22.4, 18.4, 18.3. HRMS (ESI) for $C_{82}H_{76}F_{12}N_4O_{20}Ru_4S_8$: calculated 1014.4897 $[\mathbf{4} - 2OTf]^{2+}$, 626.6757 $[\mathbf{4} - 3OTf]^{3+}$; observed 1014.4882 $[\mathbf{4} - 2OTf]^{2+}$, 626.6764 $[\mathbf{4} - 3OTf]^{3+}$. Anal. Calcd for $C_{82}H_{76}F_{12}N_4O_{20}Ru_4S_8$: C, 42.34; H, 3.29; N, 2.41. Found: C, 42.23; H, 3.10; N, 2.09.

■ ASSOCIATED CONTENT

Supporting Information

NMR, MS, UV−vis spectra, cyclic voltammograms, X-ray data, and computational details. A text file of all computed molecule Cartesian coordinates in .xyz format for convenient visualization. This material is available free of charge via the Internet at http://pubs.acs.org. CCDC reference numbers CCDC 951195 (**L1**), CCDC 951203 (**3**·PA), CCDC 951207 (*cis*-**4**·PA), and CCDC 951206 (*trans*-**4**·PA) contain the supplementary crystallographic data for this paper. These data can be obtained free of charge from the Cambridge Crystallographic Data Centre via www.ccdc.cam.ac.uk/data_request/cif.

■ AUTHOR INFORMATION

Corresponding Authors

*E-mail: bruno.therrien@unine.ch.

*E-mail: marc.salle@univ-angers.fr.

Notes

The authors declare no competing financial interest.

■ ACKNOWLEDGMENTS

The authors gratefully acknowledge the University of Angers for a grant (V.V.), and the Région des Pays de la Loire (S.B.). The PIAM (Univ. Angers) and the CRMPO (Univ. Rennes) are acknowledged for their assistance in spectroscopic analyses. The Johnson-Matthey Company is acknowledged for their generous provision of palladium salts.

■ REFERENCES

(1) (a) Cook, T. R.; Zheng, Y.-R.; Stang, P. J. *Chem. Rev.* **2013**, *113*, 734−777. (b) Ward, M. D.; Raithby, P. R. *Chem. Soc. Rev.* **2013**, *42*, 1619−1636. (c) Amouri, H.; Desmarets, C.; Moussa, J. *Chem. Rev.* **2012**, *112*, 2015−2041. (d) Klosterman, J. K.; Yamauchi, Y.; Fujita, M. *Chem. Soc. Rev.* **2009**, *38*, 1714−1725.

(2) (a) Fujita, M.; Tominaga, M.; Hori, A.; Therrien, B. *Acc. Chem. Res.* **2005**, *38*, 369−378. (b) Vajpayee, V.; Song, Y. H.; Cook, T. R.; Kim, H.; Lee, Y.; Stang, P. J.; Chi, K.-W. *J. Am. Chem. Soc.* **2011**, *133*, 19646−19649. (c) Yan, H.; Süss-Fink, G.; Neels, A.; Stoeckli-Evans, H. *J. Chem. Soc., Dalton Trans.* **1997**, 4345−4350. (d) Therrien, B.; Süss-Fink, G.; Govindaswamy, P.; Renfrew, A. K.; Dyson, P. J. *Angew. Chem., Int. Ed.* **2008**, *47*, 3773−3776. (e) Shanmugraju, S.; Vajpayee, V.; Lee, S.; Chi, K.-W.; Mukherjee, P. S. *Inorg. Chem.* **2012**, *51*, 4817−4823.

(3) (a) Barry, N. P. E.; Zava, O.; Furrer, J.; Dyson, P. J.; Therrien, B. *Dalton Trans.* **2010**, *39*, 5272−5277. (b) Smith, G. S.; Therrien, B. *Dalton Trans.* **2011**, *40*, 10793−10800. (c) Vajpayee, V.; Yang, Y. J.; Kang, S. C.; Kim, H.; Kim, I. S.; Wang, M.; Stang, P. J.; Chi, K.-W. *Chem. Commun.* **2011**, *47*, 5184−5186. (d) Vajpayee, V.; Song, Y. H.; Yang, Y. J.; Kang, S. C.; Cook, T. R.; Kim, D. W.; Lah, M. S.; Kim, I. S.; Wang, M.; Stang, P. J.; Chi, K.-W. *Organometallics* **2011**, *30*, 6482−6489. (e) Vajpayee, V.; Song, Y. H.; Jung, Y. J.; Kang, S. C.; Kim, H.; Kim, I. S.; Wang, M.; Cook, T. R.; Stang, P. J.; Chi, K.-W. *Dalton Trans.* **2012**, *41*, 3046−3052. (f) Vajpayee, V.; Lee, S.; Kim, S. H.; Kang, S. C.; Cook, T. R.; Kim, H.; Kim, D. W.; Verma, S.; Lah, M. S.; Kim, I. S.; Wang, M.; Stang, P. J.; Chi, K.-W. *Dalton Trans.* **2013**, *42*, 466−475. (g) Linares, F.; Procopio, E. Q.; Galindo, M. A.; Romero, M. A.; Navarro, J. A. R.; Barea, E. *CrystEngComm* **2010**, *12*, 2343−2346. (h) Cook, T. R.; Vajpayee, V.; Lee, M. H.; Stang, P. J.; Chi, K.-W. *Acc. Chem. Res.* **2013**, DOI: 10.1021/ar400010v. (i) Mishra, A.; Kang, S. C.; Chi, K.-W. *Eur. J. Inorg. Chem.* **2013**, 5222−5232.

(4) (a) Yamada, J.; Sugimoto, T., Eds. *TTF Chemistry. Fundamentals and Applications of Tetrathiafulvalene*; Springer Verlag: Heidelberg, 2004. (b) Special issue on molecular conductors: *Chem. Rev.* **2004**, *104*, 4887−5782. (c) Martín, N. *Chem. Commun.* **2013**, *49*, 7025−7027. (d) Bryce, M. R. *J. Mater. Chem.* **2000**, *10*, 589−598. (e) Segura, J. L.; Martín, N. *Angew. Chem., Int. Ed.* **2001**, *40*, 1372−1409.

(5) (a) Canevet, D.; Sallé, M.; Zhang, G.; Zhang, D.; Zhu, D. *Chem. Commun.* **2009**, 2245−2269. (b) Nielsen, M. B.; Lomholt, C.; Becher, J. *Chem. Soc. Rev.* **2000**, *29*, 153−164. (c) Hardouin-Lerouge, M.; Hudhomme, P.; Sallé, M. *Chem. Soc. Rev.* **2011**, *40*, 30−43.

(6) For reviews related to TTF chemistry, see: (a) Garín, J. *Adv. Heterocycl. Chem.* **1995**, *62*, 249−304. (b) Schukat, G.; Fanghanel, E. *Sulfur Rep.* **2003**, *24*, 1−190. (c) Simonsen, K. B.; Svenstrup, N.; Lau, J.; Simonsen, O.; Mørk, P.; Kristensen, G. J.; Becher, J. *Synthesis* **1996**, 407−418. (d) Jun-ichi Yamada, J.-I.; Akutsu, H.; Nishikawa, H.; Kikuchi, K. *Chem. Rev.* **2004**, *104*, 5057−5084. (e) Iyoda, M.; Hasegawa, M.; Miyake, Y. *Chem. Rev.* **2004**, *104*, 5085−5114. (f) Jeppesen, J. O.; Nielsen, M. B.; Becher, J. *Chem. Rev.* **2004**, *104*, 5115−5132. (g) Fabre, J.-M. *Chem. Rev.* **2004**, *104*, 5133−5150. (h) Gorgues, A.; Hudhomme, P.; Sallé, M. *Chem. Rev.* **2004**, *104*, 5151−5184. (i) Lorcy, D.; Bellec, N. *Chem. Rev.* **2004**, *104*, 5185−5202. (j) Lincke, K.; Nielsen, M. B. In *Organic Synthesis and Molecular Engineering*, Organic Building Blocks for Molecular Engineering; John Wiley & Sons, Inc.: 2013, pp 4−45.

(7) For recent reviews related to TTF-based ligands, see: (a) Lorcy, D.; Bellec, N.; Fourmigué, M.; Avarvari, N. *Coord. Chem. Rev.* **2009**, *253*, 1398−1438. (b) Shatruk, M.; Ray, L. *Dalton Trans.* **2010**, *39*, 11105−11121.

(8) (a) Bivaud, S.; Balandier, J.-Y.; Chas, M.; Allain, M.; Goeb, S.; Sallé, M. *J. Am. Chem. Soc.* **2012**, *134*, 11968−11970. (b) Goeb, G.; Bivaud, S.; Croué, V.; Vajpayee, V.; Allain, M.; Sallé, M. *Materials* **2014**, *7*, 611−622. (c) Goeb, S.; Bivaud, S.; Dron, P. I.; Balandier, J.-Y.; Chas, M.; Sallé, M. *Chem. Commun.* **2012**, *48*, 3106−3108. (d) Balandier, J.-Y.; Chas, M.; Goeb, S.; Dron, P. I.; Rondeau, D.; Belyasmine, A.; Gallego, N.; Sallé, M. *New J. Chem.* **2011**, *35*, 165−168. (e) Bivaud, S.; Goeb, S.; Balandier, J.-Y.; Chas, M.; Allain, M.; Sallé, M. *Eur. J. Inorg. Chem.*, DOI: 10.1002/ejic.201400060.

(9) Bivaud, S.; Goeb, S.; Croué, V.; Dron, P. I.; Allain, M.; Sallé, M. *J. Am. Chem. Soc.* **2013**, *135*, 10018−10021.

(10) (a) Govindaswamy, P.; Suss-Fink, G.; Therrien, B. *Organometallics* **2007**, *26*, 915−924. (b) Shanmugaraju, S.; Samanta, D.; Mukherjee, P. S. *Beilstein J. Org. Chem.* **2012**, *8*, 313−322.

(11) Mitamura, Y.; Yorimitsu, H.; Oshima, K.; Osuka, A. *Chem. Sci.* **2011**, *2*, 2017−2021.

(12) Brooks, A. C.; Day, P.; Dias, I. G.; Rabaça, S.; Santos, I. C.; Henriques, R. T.; Wallis, J. D.; Almeida, M. *Eur. J. Inorg. Chem.* **2009**, 3084−3093.

(13) Frisch, M. J.; et al. *Gaussian03*, Revision B.04; Gaussian: Pittsburgh, PA, 2003.

(14) Xunwen, X.; Guannan, W.; Liangjun, S.; Jianghua, F.; Haoqi, G. *Synth. Met.* **2012**, *162*, 900−903.

(15) Johnson, C.D. *The Hammett Equation*; Cambridge University Press: Cambridge, 1980.

(16) Cohen, Y.; Avram, L.; Frish, L. *Angew. Chem., Int. Ed.* **2005**, *44*, 520−554.